Analyst

PAPER

View Article Online
View Journal

Cite this: DOI: 10.1039/d5an01187f

Digital fluorescent pH probes: polymer-based design, fluorescence response, mechanism, functional tuning and application to logic operation in live cells

Seiichi Uchiyama, * Eiko Hamada, Masaharu Takarada and Kohki Okabe

We report fluorescent digital pH probes based on a polymeric design comprising thermoresponsive, proton-binding and environment-sensitive fluorescent units. At selected temperatures, fluorescence switching was nearly complete, with a slight pH variation of <1 unit. The fluorescence-switching mechanism involved a proton-induced three-dimensional structural change in the polymer, which altered local hydrophobicity near the environment-sensitive fluorescent units. Based on the change in local hydrophobicity during operation, extremely sharp responses were produced because of the variation in proton-binding abilities of the probes. The polymeric design ensured functional flexibility, including a pH-responsive region and a direction of fluorescence switching. As an application of fluorescent digital pH probes, intracellular logic operations were performed by varying the pH and temperature. By distinguishing the minute pH and temperature difference inside mammalian cells, a specific condition—high pH and temperature—generated strong fluorescence with an extended fluorescence lifetime, as confirmed *via* fluorescence-lifetime imaging microscopy.

Received 9th November 2025,
Accepted 5th February 2026

DOI: 10.1039/d5an01187f

rsc.li/analyst

Introduction

Fluorescent probes change their fluorescence characteristics such as fluorescence intensity and lifetime, and maximum emission wavelength in response to concentrations of chemical species (*i.e.*, ions or molecules) or variations in physical quantities (*e.g.*, temperature and viscosity).[1–3] To date, various fluorescent ion probes have been developed. Among them, fluorescent pH probes are used in specialized research areas and even daily life,[4] as aqueous solutions always contain protons, and solution pH predominantly influences chemical reactions[5] and bioenergetically represented biological events.[6] Fluorescence-imaging microscopy is a practical application of fluorescent pH probes, with a significant impact on biology.[7]

As a general principle of fluorescent ion probes, the function of fluorescent pH probes relies on the equilibrating complexation of the receptor (*e.g.*, an amine) and target ion (*i.e.*, the proton in this case) (eqn (1)).

$$\text{Free probe} + \text{H}^+ \rightleftarrows \text{Protonated probe} \quad (1)$$

The difference between free and protonated receptors in their effects on the electric properties of the fluorophore is the basis of the fluorescence off–on switching mechanism. The control of internal charge transfer (ICT) and photoinduced electron transfer (PET) efficiency is involved in fluorescent pH probes.[8] The definition of the acidity constant (K_a) for a fluorescent pH probe is expressed as eqn (2).

$$K_a = ([\text{Free probe}][\text{H}^+])/[\text{Protonated probe}] \quad (2)$$

The following eqn (3) should always be effective in an aqueous solution.

$$-\log([\text{Protonated probe}]/[\text{Free probe}]) = \text{pH} - \text{p}K_a \quad (3)$$

Eqn (3) indicates that the operational pH width of probes is fundamentally constant (two pH units are necessary for the variation from [Protonated probe]/[Free probe] = 0.1 to [Protonated probe]/[Free probe] = 10), whereas the operational pH range shifts according to the pK_a value of the probe.

Although the relation in eqn (3) is universal for fluorescent pH probes, unusually sharp responses to pH variation in a narrow pH width appear in considerably limited cases, involving inner filter effects,[9] micellization of block copolymers,[10–12] deoxyribonucleic acid (DNA) i-motifs[13] and sequential protonation of multiple receptors in a molecule.[14–16] Such digital responses of fluorescent pH probes are beneficial for highly sensitive pH monitoring and molecular logic operation,[17–20] where fluorescence switching should be completed by a minor variation in proton concentrations (a small pH change). A note-

Graduate School of Pharmaceutical Sciences, The University of Tokyo, 7-3-1 Hongo, Bunkyo-ku, Tokyo 113-0033, Japan. E-mail: seiichi@g.ecc.u-tokyo.ac.jp

worthy application of a digital fluorescent pH-sensing system is highly selective *in vivo* tumor imaging in mice.[21]

In 2009, we unexpectedly discovered the digital behavior of a few fluorescent polymeric pH probes and reported four examples in a preliminary communication.[22] Our detailed findings are mentioned here again. (i) Poly(*N*-isopropylacrylamide) (PNIPAM) is a thermoresponsive polymer with a lower critical solution temperature (LCST)[23,24] and forms a flexible structure upon hydration between the amide groups of NIPAM units and solvent water molecules in cold aqueous solutions. In contrast, it becomes rigid and globular by the breaking of hydrogen bonds and the accompanying entropy gain due to the released water molecules when the temperature of the solution is >31 °C (*i.e.*, the LCST of PNIPAM).[25] The hydrophobic interaction between isopropyl moieties in side chains is dominant, forming relatively large interpolymeric agglomerates. Thus, the solution becomes colloidal when the temperature is >31 °C (Fig. 1a).[23] (ii) When ion-binding units are incorporated into PNIPAM, the copolymer responds to ions and temperature changes. The LCST of the copolymer containing the benzo-18-crown-6 moiety depends on the K^+ concentration (Fig. 1b).[26] At high K^+ concentrations, benzo-18-crown-6 forms an ionic K^+ complex, decreasing the hydrophobicity of the side chain and shifting the LCST to a high temperature. Thus, the copolymer comprising benzo-18-crown-6 is considered a polymeric K^+ probe in aqueous solution when the temperature is fixed between the two LCSTs. (iii) A small amount of an environment-sensitive (polarity- and hydrogen-bonding-sensitive) fluorophore is incorporated into PNIPAM to form a copolymer, which functions as a fluorescent thermometer. The copolymer comprising NIPAM and *N*-{2-[(7-*N*,*N*-dimethylaminosulfonyl)-2,1,3-benzoxadiazol-4-yl](methyl)

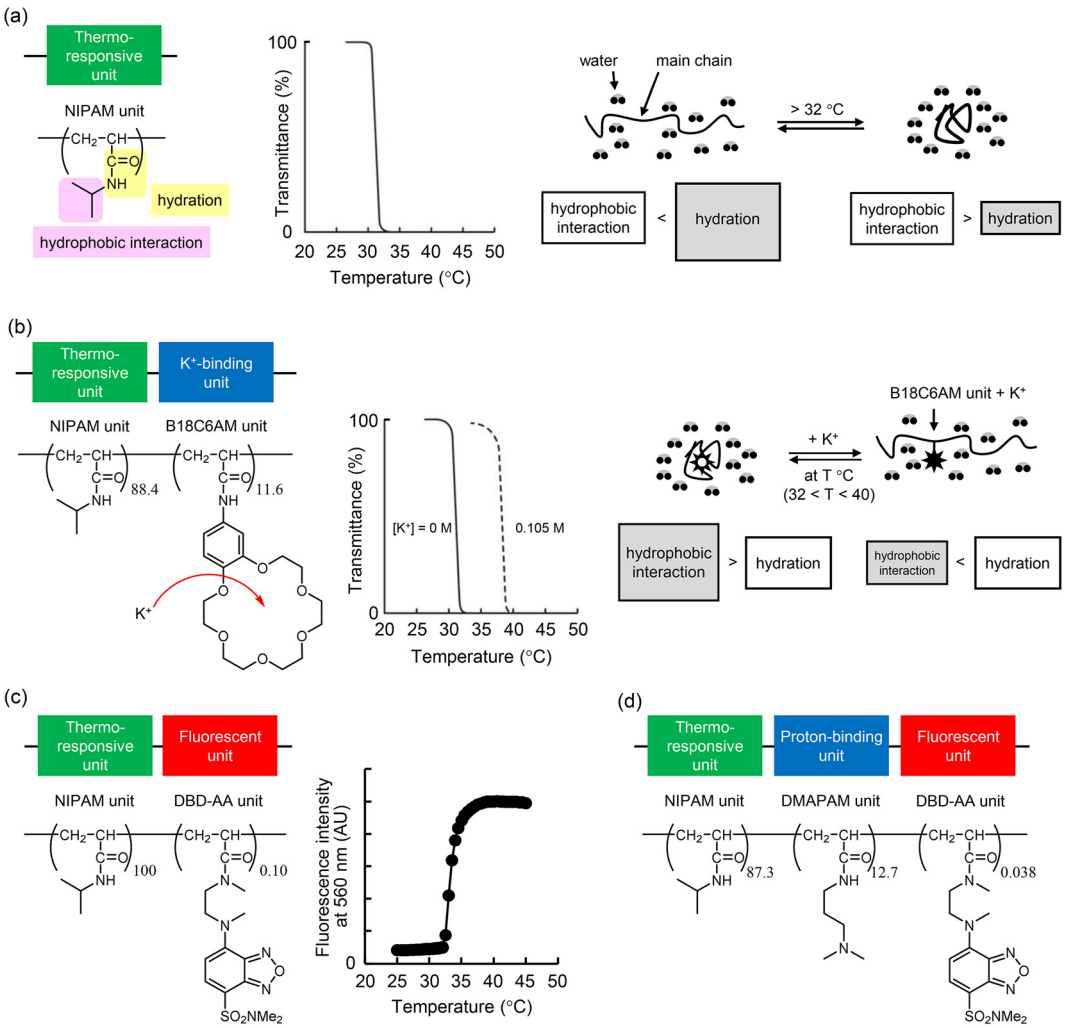

Fig. 1 Thermoresponsive-PNIPAM-based functional polymers. (a) PNIPAM. Chemical structure (left), temperature-dependent transmittance of the aqueous solution (1 wt%) (middle), and operational mechanism (right). (b) Poly(NIPAM-*co*-B18C6AM). Chemical structure (left), [K^+]-dependent transmittance of the aqueous solution (1 wt%) ([K^+] = 0 or 0.105 mol L^{-1}) (middle), and operational mechanism (right). (c) Poly(NIPAM-*co*-DBD-AA). Chemical structure (left) and temperature-dependent fluorescence intensity of the heated aqueous solution (0.01 w/v%) (right, measured using the procedure described in ref. 27). The excitation wavelength is 456 nm. (d) Chemical structure of poly(NIPAM-*co*-DMAPAM-*co*-DBD-AA) (copolymer **1**). Transmittance changes in panels (a) and (b) are adapted with permission from ref. 23 and 26, respectively.

amino}ethyl-*N*-methylacrylamide (DBD-AA) [poly(NIPAM-*co*-DBD-AA)] emits strong fluorescence when the solution temperature is increased beyond the LCST (>31 °C) (Fig. 1c).[27] Fluorescent polymeric thermometers developed based on this strategy play a crucial role in monitoring intracellular temperature.[28] Additionally, the concept of thermal signaling[29] has been proposed by using fluorescent polymeric thermometers in cellular biology. (iv) We predicted a fluorescent polymeric pH probe when proton-binding and environment-sensitive fluorescent units were incorporated into PNIPAM. The copolymer comprising NIPAM, *N*-[3-(dimethylamino)propyl]acrylamide (DMAPAM) and DBD-AA units [poly(NIPAM-*co*-DMAPAM-*co*-DBD-AA), **1**; Fig. 1d] showed pH-dependent fluorescence characteristics, and for some reason, the response was much sharper than that of conventional fluorescent pH probes.[22]

This article is a full paper version based on the previous work.[22] In the beginning, the fluorescence characteristics of **1** are described for the second time to demonstrate its unusually sharp response to a pH variation. Then, we elucidate the functional mechanism underlying high sensitivity to small pH variations. The structural flexibility and limitations of digital fluorescent pH probes for tuning the operational pH range (pK_a of the probe) and the switching direction (*i.e.*, on–off *vs.* off–on) are discussed using new and reported polymers.[22] Finally, the digital fluorescent pH probes are applied to molecular logic operations that can simultaneously sense multiple chemical and physical factors in live cells. Extremely sharp responses to pH and temperature enable the discrimination of a specific cellular status, with slight pH and temperature differences.

Experimental

Materials

N-(3-Aminopropyl)acrylamide (APAM),[30] DBD-AA,[27] 4-(2′-*N*,*N*-dimethylaminoethyl)amino-7-*N*,*N*-dimethylaminosulfonyl-2,1,3-benzoxadiazole (DBD-DMAEA),[31] *N*,2-dimethyl-*N*-(2-{methyl[7-(dimethylsulfamoyl)-2,1,3-benzoxadiazol-4-yl]amino}ethyl)propanamide (DBD-IA),[32] *N*-[3-(diethylamino)propyl]acrylamide (DEAPAM),[22] *N*-(3-morpholin-4-ylpropyl)acrylamide (MPAM),[22] *N*-*n*-propylacrylamide (NNPAM),[33] and 4-vinylbenzoic acid (VBA)[34] were prepared using reported methods. NIPAM was obtained from Wako Pure Chemicals (currently, FUJIFILM Wako Pure Chemical Corporation) and purified *via* recrystallization from *n*-hexane. DMAPAM was obtained from Wako Pure Chemicals. HPTS was purchased from Invitrogen (currently, Thermo Fisher Scientific, Inc.). *N*-*tert*-Butylacrylamide (NTBAM) was obtained from Sigma-Aldrich. Water was purified using a Milli-Q® reagent system (Direct-Q 3 UV, Millipore). All other reagents were of guaranteed reagent grade and used without further purification.

Synthesis of dimethyl 2,2′-((3-acrylamidopropyl)azanediyl) diacetate (DMAcAPAM)

APAM (as hydrochloric acid salt, 165 mg, 1 mmol) and potassium carbonate (742 mg) were suspended in acetonitrile (10 mL). After the addition of methyl bromoacetate (918 mg, 6 mmol), the mixture was stirred at 70 °C for 6 h. After the reaction, the solution was filtered and evaporated under reduced pressure. The residue was chromatographically separated on a silica gel column using dichloromethane–methanol (100 : 1, v/v) as an eluent to produce DMAcAPAM as a colorless oil (48.4 mg, 17.8%); ^{1}H NMR (400 MHz, $CDCl_3$, δ): 7.68 (br, 1H), 6.28–6.33 (ss, 1H, J = 2.6, 17.0 Hz), 6.20–6.26 (ss, 1H, J = 9.4, 17.0 Hz), 5.58–5.61 (d, 1H, J = 2.6, 9.4 Hz), 3.72 (s, 6H), 3.47–3.52 (m, 6H), 2.78 (t, 2H, J = 5.8 Hz), 1.63–1.69 (m, 2H); ^{13}C NMR (100 MHz, $CDCl_3$, δ): 171.9, 165.6, 131.5, 125.5, 54.7, 52.2, 51.8, 37.8, 25.9; HRMS-ESI (m/z): [M + Na^+] calcd for $C_{12}H_{20}N_2NaO_5^+$: 295.1264; found: 295.1264.

Preparation of copolymers

General procedures for preparing 1–6. NIPAM (4.5 mmol), a proton-binding monomer (DMAPAM, DEAPAM, MPAM, DMAcAPAM, acrylic acid (AA) or VBA; 0.5 mmol), DBD-AA (5 μmol) and α,α′-azobisisobutyronitrile (AIBN, 50 μmol) were dissolved in 1,4-dioxane (10 mL). The solution was bubbled with dry nitrogen or argon for 30 min to remove dissolved oxygen. The reaction mixture was polymerized at 60 °C for 6–8 h (6 h for **2–4** and **6**, and 8 h for **1** and **5**), cooled to room temperature, and poured into diethyl ether (200 mL). The obtained copolymer was purified *via* reprecipitation using 1,4-dioxane (10 mL) and diethyl ether (200 mL). The yields are summarized in Table 1.

Preparation of 7 and 8. NNPAM or NTBAM (4.5 mmol), DMAPAM (0.5 mmol), DBD-AA (5 μmol) and AIBN (50 μmol) were dissolved in 1,4-dioxane (10 mL). The solution was then bubbled with dry argon to remove dissolved oxygen. The reaction mixture was polymerized at 60 °C for 6 h, cooled to room temperature, and poured into diethyl ether (200 mL; for **7**) or *n*-hexane (200 mL; for **8**). The obtained copolymer was purified *via* reprecipitation using acetone (5 mL)–diethyl ether (150 mL) for **7** or acetone (5 mL)–*n*-hexane (200 mL) for **8**. The yields are summarized in Table 1.

Fluorescent polymeric logic gate 9. NIPAM (2.25 mmol), MPAM (0.25 mmol), DBD-AA (25 μmol) and AIBN (25 μmol) were dissolved in 1,4-dioxane (5 mL), and the solution was bubbled with dry argon for 30 min to remove dissolved oxygen. The reaction mixture was polymerized at 60 °C for 6 h, cooled to room temperature, and poured into diethyl ether (100 mL). The obtained copolymer was purified *via* reprecipitation using 1,4-dioxane (5 mL) and diethyl ether (100 mL). The yield was 63%.

Characterization of copolymers

The thermoresponsive and proton-binding units in the copolymers, except for copolymer **5**, were characterized by ^{1}H-nuclear magnetic resonance (^{1}H-NMR) spectra recorded using Bruker Avance III HD 400 in deuterated chloroform ($CDCl_3$). The content of AA units in **5** was determined by an acid–base titration. The proportions of DBD-AA units in the copolymers were determined from the absorbance in methanol, which was com-

Table 1 Characterization of the synthesized copolymers composed of thermoresponsive, proton-binding and fluorescent DBD-AA units

No.	Thermo-responsive unit	Proton-binding unit	Feed ratio[a]	Yield (%)	Actual unit ratio[b]	M_w[c]	M_n[d]	M_w/M_n
1[e]	NIPAM	DMAPAM	90 : 10 : 0.1	83	87.3 : 12.7 : 0.038	120 000	40 000	3.01
2[e]	NIPAM	DEAPAM	90 : 10 : 0.1	71	92.2 : 7.8 : 0.028	79 500	39 200	2.03
3[e]	NIPAM	MPAM	90 : 10 : 0.1	82	90.8 : 9.2 : 0.066	70 300	23 200	3.03
4	NIPAM	DMAcAPAM	90 : 10 : 0.1	67	92.5 : 7.5 : 0.092	82 800	34 000	2.44
5[e]	NIPAM	AA	90 : 10 : 0.1	83	90.9 : 9.1 : 0.079	139 000	56 700	2.45
6	NIPAM	VBA	90 : 10 : 0.1	56	86.1 : 13.9 : 0.091	16 500	11 300	1.46
7	NNPAM	DMAPAM	90 : 10 : 0.1	63	90.7 : 9.3 : 0.054	108 000	47 200	2.29
8	NTBAM	DMAPAM	90 : 10 : 0.1	62	90.2 : 9.8 : 0.068	78 800	34 700	2.27
9	NIPAM	MPAM	90 : 10 : 1	63	91.2 : 8.8 : 0.77	118 000	55 500	2.12

[a] Ratio of monomers for thermoresponsive, proton-binding and fluorescent DBD-AA units. [b] Ratio of thermoresponsive, proton-binding and fluorescent DBD-AA units. [c] Weight-average molecular weight. [d] Number-average molecular weight. [e] Originally reported in ref. 22.

pared with that of the model fluorophore DBD-IA [molar absorption coefficient (ε) = 10 800 M^{-1} cm^{-1} at 444 nm].[32]

The molecular weights of the copolymers were determined *via* gel permeation chromatography (GPC), comprising a JASCO PU-4580 pump, a JASCO RI-4030 refractive index detector, a JASCO CO-4060 column thermostat (set at 40 °C) and a Shodex GPC KD-806M column. A calibration curve was generated using a polystyrene standard, and 1-methyl-2-pyrrolidinone containing lithium bromide (LiBr; 20 mM) was used as the eluent.

Fluorescence measurements of copolymers

The fluorescence spectra of the copolymers were recorded using a JASCO FP-6500 spectrofluorometer—equipped with a Hamamatsu R-7029 optional photomultiplier tube (operative range: 200–850 nm)—or a JASCO FP-8500 spectrofluorometer—equipped with a Hamamatsu R928 optional photomultiplier tube (operative range: 200–850 nm)—in Britton–Robinson buffer solutions[35] with excitation at 450 nm, and corrected using a JASCO ESC-333 standard light source. Borate (0.1 M),[36] phosphate (0.2 M)[37] and citrate (0.2 M)[38] buffer solutions were also used for evaluating the functions of **1**, **3** and **5**, respectively. After adjusting the pH at 20 °C, the sample was equilibrated at a specific temperature for at least 60 s. The sample temperature was controlled using a JASCO ETC-273T temperature controller. The fluorescence quantum yields (Φ_f) were determined using a JASCO FP-8500 spectrofluorometer with a JASCO ILF-835 integrating sphere unit.

The fluorescence lifetimes were measured using a Horiba Jobin Yvon FluoroCube 3000U. The samples were excited at 456 nm with an LED (NanoLED-460, Horiba) at a repetition rate of 1 MHz. The temperature of the sample was controlled using a JASCO ETC-273T temperature controller. The obtained fluorescence decay curve was fitted by a double-exponential function using eqn (4).

$$I(t) = A_1 \exp(-t/\tau_1) + A_2 \exp(-t/\tau_2) \quad (4)$$

Fractional contributions (P_1 and P_2 for τ_1 and τ_2, respectively) and average fluorescence lifetimes were calculated using the following equations:

$$P_1 = A_1\tau_1/(A_1\tau_1 + A_2\tau_2) \times 100 \quad (5)$$

$$P_2 = A_2\tau_2/(A_1\tau_1 + A_2\tau_2) \times 100 \quad (6)$$

$$\tau_f = (A_1{\tau_1}^2 + A_2{\tau_2}^2)/(A_1\tau_1 + A_2\tau_2) \quad (7)$$

Determination of pK_a for the conjugate acid of the dimethylmonoalkylamino moiety

The pK_a value of the conjugate acid of the dimethylmonoalkylamino moiety was determined *via* pH titration of the model fluorescent pH probe, DBD-DMAEA, exhibiting PET control-based fluorescence off–on switching. The apparent pK_a values ($_{app}$pK_a) of DBD-DMAEA were determined in pure water, mixtures of water and methanol (4 : 1, 1 : 1 and 1 : 4 w/w), and mixtures of water and ethanol (4 : 1, 1 : 1 and 1 : 4 w/w) by fitting the pH values measured using a glass electrode (9618S-10D, Horiba)-equipped pH meter (LAQUA F-73, Horiba) and pH-dependent fluorescence intensity data using eqn (8).

$$-\log[(FI_{max} - FI)/(FI - FI_{min})] = pH - {}_{app}pK_a \quad (8)$$

where FI is the observed fluorescence intensity at a fixed wavelength, FI_{max} and FI_{min} are the corresponding maximum and minimum fluorescence intensities, respectively, and $_{app}$pK_a is the apparent acidity constant. In alcohol-containing solutions, pK_a values were obtained by subtracting the liquid-junction potential (δ)[39,40] (Table 2) from $_{app}$pK_a values.

Logic operation in live HeLa cells

Fluorescence lifetime imaging was performed using a Leica TCS SP8-FALCON confocal laser scanning microscope with a time-correlated single photon counting (TCSPC) module. Cultured HeLa cells were washed with phosphate-buffered saline (PBS) and then treated with a 5% glucose solution containing 0.05 w/v% of **9**. After incubation at room temperature for 10 min, the cells were washed twice with PBS and immersed in 50 mM phosphate buffer solutions (pH 5.5–8.0) containing 80 mM potassium chloride, 1 mM magnesium chloride and 20 μM nigericin.[41] The treated HeLa cells were allowed to stand at room temperature for 5 min and observed at fixed temperatures under excitation by a PicoQuant PDL 800-B pulsed laser at 470 nm with a repetition rate of 20 MHz. The temperature of the microscope stage was controlled using Tokai Hit STXG-WSKMX-SET. Fluorescence emitted in the

Table 2 pK_a values of the protonated tertiary amine of DBD-DMAEA in various aqueous solvents

Solvent	D^a	$_{app}pK_a{}^b$	δ^c	pK_a
Water	78.5	8.35	—	8.35
Water–methanol (8 : 2, w/w)	69.2	8.01	0.01	8.00
Water–methanol (5 : 5, w/w)	54.9	7.52	0.13	7.39
Water–methanol (2 : 8, w/w)	40.1	6.84	−0.06	6.90
Water–ethanol (8 : 2, w/w)	67.0	7.98	−0.03	8.01
Water–ethanol (5 : 5, w/w)	49.0	7.25	0.17	7.08
Water–ethanol (2 : 8, w/w)	32.8	6.72	0.11	6.61

[a] Dielectric constant.[76] [b] Measured using a glass electrode pH meter standardized as per usual using aqueous buffer solutions. [c] Correction constant for a specific composition of a solvent medium.[40]

500–700 nm range was captured, using an HC PL APO 63 × 1.40 NA oil CS2 objective lens (Leica) in 512 × 512 pixel format, with a pinhole size of 3 units. Samples were scanned at 400 Hz and fluorescence lifetime images were acquired by accumulating 50 times. To achieve a photon count rate of 0.5%–2% of the pulse count rate (2×10^7 Hz), the laser power was controlled. Fluorescence lifetime images were obtained using Leica Application Suite X in a fast FLIM mode.

Results and discussion

Digital fluorescence responses of 1 to pH variations

First, the function of **1** as a fluorescent pH probe were demonstrated. The copolymers studied herein were prepared *via* random polymerization using AIBN. The characterization of unit compositions and molecular weights of the as-prepared copolymers are summarized in Table 1. The unit ratios of thermoresponsive, proton-binding and fluorescent units in the copolymers were equivalent to the corresponding monomer ratios in the feed. Fig. 2a shows the relation between the fluorescence intensity of **1** and temperature in Britton–Robinson buffer solutions at pH 2 and 12.[42] The DMAPAM units in **1** are expected to be protonated at pH 2 and deprotonated at pH 12. Fig. 2a (closed circle) shows NIPAM units-induced thermoresponsive behavior of **1** at pH 12. In contrast, this behavior disappeared at pH 2 (open circle), as protonated **1** is too hydrophilic to be subjected to a heat-induced phase transition. The orange region shown in Fig. 2a suggests that the fluorescence off–on switching of **1** is induced by changing pH values in the range of approximately 45 °C–60 °C.

Fig. 2b displays the fluorescence response of **1** to a pH variation. When the solution temperature was 50 °C (closed circle), the fluorescence intensity was pH dependent. The corresponding pH-dependent fluorescence spectra at 50 °C are shown in Fig. 2c. However, no fluorescence switching was observed when the solution temperature was 20 °C (open circle, Fig. 2b). Fig. 2a clarifies the difference between the fluorescence-switching behavior at 20 °C and 50 °C. Notably, the response curve of **1** at 50 °C to pH variation was remarkably sharp. Fluorescence switching of **1** was completed in a narrower pH range than those of conventional organic fluorescent pH probes. The

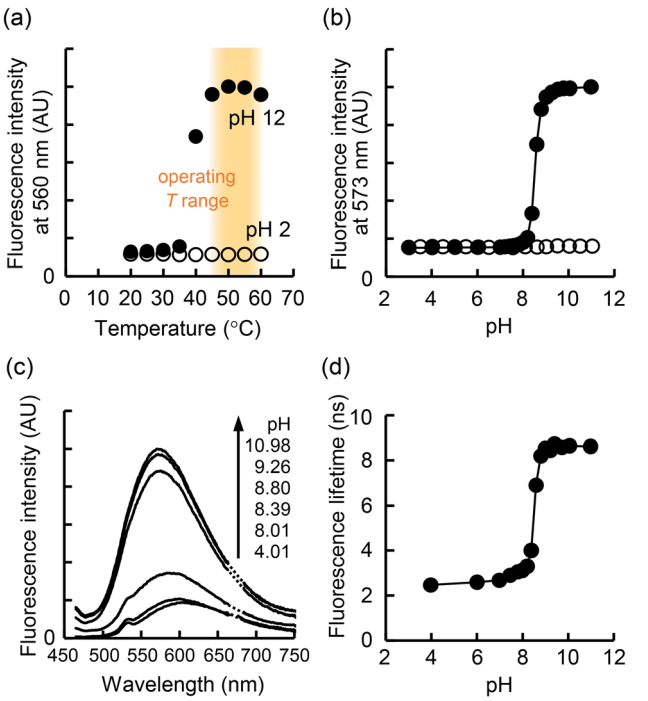

Fig. 2 Fluorescence characteristics of copolymer **1** (0.01 w/v%) in Britton–Robinson buffer solutions. (a) Fluorescence responses to temperature variation at pH 12 (closed) and 2 (open) with increasing temperature. (b) Fluorescence responses to pH variation at 50 °C (closed) and 20 °C (open). (c) The pH-dependent fluorescence spectra recorded at 50 °C. In the dotted-line region, excitation light-induced scattering overlaps with the fluorescence spectra. (d) The pH-dependent fluorescence lifetime at the maximum emission wavelength at 50 °C. Samples were excited at 450 nm for (a)–(c) and 456 nm for (d).

response curve of 8-hydroxypyrene-1,3,6-trisulfonate (HPTS)[43] (Fig. S1) is a representative of the latter pH probes.

To analyze the unusual pH-dependent fluorescence behavior of **1**, we introduced an extended relation (eqn (9)), based on the Henderson–Hasselbalch equation.[44]

$$-\log[(FI_{max} - FI)/(FI - FI_{min})] = a\ (pH - pK_a) \qquad (9)$$

where FI is the observed fluorescence intensity at a fixed wavelength, FI_{max} and FI_{min} are the corresponding maximum and minimum fluorescence intensities, respectively, pK_a is the (apparent) acidity constant, and a is the slope (equivalent to one for conventional fluorescent pH probes following the original Henderson–Hasselbalch equation). The fluorescence response parameters of **1** to pH variation at 50 °C are a = 3.69 ± 0.34 and pK_a = 8.68 ± 0.08 [average ± standard deviation (s.d.)] in Britton–Robinson buffer solutions.[45] In a reference experiment, a conventional fluorescent pH probe (HPTS) shows a = 1.01 ± 0.02 and pK_a = 7.42 ± 0.01. According to eqn (9), a high a value indicates that a small pH variation is sufficient for the complete fluorescence off–on switching of a pH probe. The pH variation required for the fluorescence output to change from 90.9% to 9.09% for **1** at 50 °C is only 0.52 units (*cf.*, conventional fluorescent pH probes including

Table 3 Fluorescence properties of the synthesized copolymers composed of thermoresponsive, proton-binding and fluorescent DBD-AA units in Britton–Robinson buffer solutions; the maximum emission wavelength (λ_{em}), fluorescence quantum yield (Φ_f), fluorescence lifetime (τ_f), fluorescence rate constant (k_f) and nonradiative rate constant (k_{nr})

Copolymer	State	pH	T (°C)	λ_{em} [a]/nm	Φ_f	τ_f [b]/ns	$k_f/10^7$ s^{-1}	$k_{nr}/10^7$ s^{-1}
1	Off	7	50	605	0.046	3.3	1.4	29.2
	On	11	50	574	0.20	9.8	2.1	8.2
2	Off	7	40	600	0.033	3.2	1.0	30.1
	On	11	40	570	0.20	10.4	1.9	7.7
3	Off	4	50	601	0.084	3.0	2.8	30.9
	On	8	50	570	0.28	9.8	2.9	7.4
4	Off	2	40	602	0.057	3.0	1.9	31.6
	On	6	40	571	0.30	10.1	3.0	6.9
5	Off	6	45	600	0.042	2.9	1.5	33.3
	On	2	45	560	0.34	12.8	2.7	5.1
6	Off	6	20	601	0.044	8.5	0.5	11.2
	On	2	20	553	0.37	18.2	2.0	3.5
7	Off	7	37	600	0.086	3.7	2.3	24.7
	On	11	37	568	0.25	10.2	2.4	7.4

[a] Excited at 450 nm and corrected. [b] Average fluorescence lifetimes at λ_{em}. Calculated using double-exponential components (Table S4) and eqn (7).

HPTS always require two pH units). Herein, a fluorescent pH probe with a high a value is called a digital fluorescent pH probe, which exhibits a digital-type sharp response curve in the pH-fluorescence output signal diagram. The maximum emission wavelength of DBD-AA units in **1** is hypsochromically shifted with increasing pH (Fig. 2c), indicating that the microenvironment near DBD-AA units changes from hydrophilic to hydrophobic because of the three-dimensional structural change in the copolymer.

The fluorescence lifetime is a valuable detection parameter, especially in bioimaging, because it is independent of the fluorophore concentration and excitation source strength.[46] Fig. 2d shows the pH-dependent fluorescence lifetime of **1** at 50 °C, calculated based on the corresponding fluorescence decay curve fitted using a double-exponential function (Table S1). A related study using poly(NIPAM-*co*-DBD-AA)[32] suggests that double components in the fluorescence decay curves of **1** correspond to the fluorophore (DBD-AA units) with and without hydrogen bonding to water molecules. Similar to fluorescence intensity (Fig. 2b), the fluorescence lifetime of **1** at 50 °C sharply responded to a pH variation in a narrow range, yielding a = 3.12 and apparent pK_a = 8.47 according to eqn (9), where the fluorescence intensity data are replaced by the average fluorescence lifetime data (Fig. 2d). The pK_a (8.47) of copolymer **1** calculated based on fluorescence lifetime measurements is slightly lower than the pK_a (8.68) obtained by measuring the fluorescence intensity because of the mathematical weighing of components in obtaining these values. The fluorescence properties of **1** in the fluorescence "off" and "on" states are summarized in Table 3.

Mechanism of 1 for producing sharp fluorescence responses to a pH variation

The mechanism of exceptional digital-type responses to a pH variation was investigated. **1** functions as a fluorescent pH probe because of the three-dimensional structural change that occurs owing to the variation in hydrophobicity/hydrophilicity of proton-binding units. This is entirely different from that of conventional small organic fluorescent pH probes, which are based on the electronic effects of an acid–base equilibrium on a fluorophore. Thus, we hypothesized that the simultaneous two physicochemical variations according to the pH-dependent polymeric structural change in **1** were involved in the digital-type responses: (i) microenvironmental polarity near the main chain of **1** and (ii) basicity of amino moieties in DMAPAM units in **1**. Therefore, we experimentally investigated these physicochemical variations during the operation of **1**.

Fig. 3a displays the pH-dependent maximum emission wavelength (left axis) of **1** at 50 °C. Because the maximum emission wavelength of DBD-IA (Fig. 3b), a model of a DBD-AA unit, correlates well with the dielectric constant (D) of solvent (Table S2 and Fig. S2),[47] the pH-dependent microenvironmental polarity near **1** during its function can be evaluated based on the maximum emission wavelength as a local D (right axis; Fig. 3a). Thus, the local D values near **1** are 58 and 7 in acidic and basic pH regions, respectively.

The basicity of the dimethylalkylamino group in DMAPAM units in **1** under high or low polarity was assessed using DBD-DMAEA[31] (Fig. 3c) as a fluorescent pH probe bearing the identical dimethylalkylamino moiety. The fluorescence off–on switching principle of DBD-DMAEA is based on the control of PET,[48] and the pK_a value of the conjugate acid of DBD-DMAEA in water can be determined *via* fluorescence titration with varying pH (Fig. S3). Similarly, the pK_a values of the conjugate acid of DBD-DMAEA in various media with different polarities were obtained using mixtures of water–methanol and water–ethanol (Table 2 and Fig. 3d). Fig. 3d shows that the basicity of the dimethylalkylamino moiety in DBD-DMAEA is reduced when the environmental polarity decreases. Limited reports on the decrease in pK_a values for amines with decreasing environmental polarity are found for aniline,[49] pyridine,[49] 1-benzylimidazole[50] and propranolol.[50]

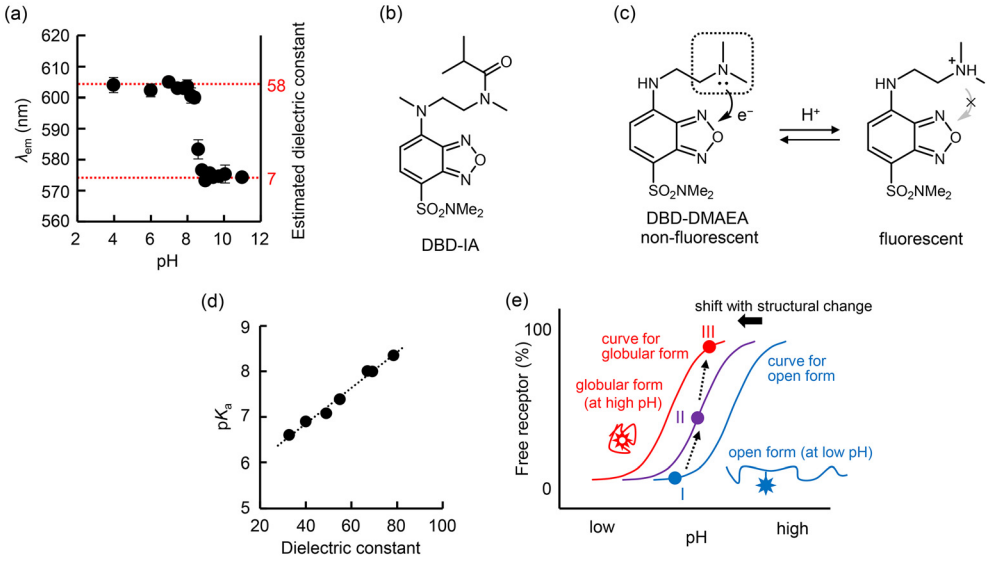

Fig. 3 Digital fluorescence response mechanism of copolymer **1**. (a) Relationship between the maximum emission wavelength (λ_{em}) of copolymer **1** (average ± s.d.) and pH at 50 °C in Britton–Robinson buffer solutions. The maximum emission wavelength can be converted to the local dielectric constant at the DBD-AA unit's location (see the main text). (b) Chemical structure of DBD-IA. (c) Scheme of a PET-based fluorescent pH probe, DBD-DMAEA, used for evaluating the polarity-dependent basicity of the tertiary amino group. (d) Relationship between the pK_a for the conjugate acid of DBD-DMAEA and the dielectric constant of the solvent. (e) A virtual shift in the fluorescence response curve, which copolymer **1** follows. This shift represents the digitalization of the response, in which the pK_a of the amino group (*i.e.*, the receptor) in copolymer **1** depends on the pH during operation.

Fig. 3e explains the sharp fluorescence responses of **1** to pH variations. In an acidic solution (low pH), **1** is extended by protonated DMAPAM units, where local polarity is relatively high near the copolymer, and the fluorescence response follows the rightmost (blue) curve with a relatively high pK_a. With increasing pH, protonated DMAPAM units are gradually neutralized, shrinking **1** and reducing the microenvironmental polarity near it. The fluorescence response curve is shifted leftward (purple line), accompanying a moderate pK_a. In an alkaline (high pH) solution, the basicity of the dimethylalkylamino moiety in DMAPAM units further decreases because of the low microenvironmental polarity, and the fluorescence response curve shifts further left (red line). Thus, the digital fluorescence response curve of **1** is produced by moving on these shifting response curves with the pH-dependent pK_a values of proton receptors (I → II → III, Fig. 3e).

Modulation of the operational pH range and switching direction of digital fluorescent polymeric pH probes

The elucidated operational mechanism of **1** enables the development of digital fluorescent polymeric pH probes that operate in various pH ranges by replacing DMAPAM units with different proton-binding units. Copolymers **2**–**4** contain amino moieties with different basicities: DEAPAM units in **2**, MPAM units in **3** and DMAcAPAM units in **4** in the decreasing order of basicity of an amino group (Fig. 4a–c). The pK_a values of conjugate acids of DEAPAM and MPAM in water are 10.3 and 7.0, respectively.[51] Due to the electron-withdrawing CH_2COOMe group of DMAcAPAM units, the pK_a value of the conjugated acid of DMAcAPAM is further reduced.[52] Fig. 4a–c show the fluorescence responses of **2**–**4** to pH variations in Britton–Robinson buffer solutions at the predetermined fixed functional temperatures (Fig. S4a–c). Ideally, **2** (a = 4.15 ± 0.59; pK_a = 9.13 ± 0.04), **3** (a = 2.54 ± 0.04; pK_a = 6.16 ± 0.03), and **4** (a = 3.95 ± 0.29; pK_a = 3.03 ± 0.01) displayed sharp digital responses in different operational pH ranges, depending on amino group basicity in proton-binding units.[53] The tunable operational pH range is a distinct advantage of our polymeric design for digital fluorescent pH probes.

The fluorescence off–on switching direction can also be reversed by replacing the proton-binding amino units in digital fluorescent polymeric pH probes with carboxylic acids. Copolymer **5** contains AA units as proton-releasing structures. After evaluating its functional temperature range (Fig. S4d), **5** showed a sharp fluorescence response to pH variation ($|a|$ = 4.29 ± 0.38; pK_a = 5.16 ± 0.14) in Britton–Robinson buffer solutions at 45 °C (Fig. 4d).[54] Strong fluorescence appeared in the low pH region (in this switching direction, a in eqn (9) is negative). In contrast to proton-binding amino units, AA units in **5** are less polar in a high-acidic pH range to take the shrinking polymeric structure. Similar to the cause of the extreme sharp fluorescence responses of **1**, the polarity-dependent acidity of the carboxylic group in AA units[55] is likely a secret of the digital-type fluorescence responses of **5**.

Copolymer **6** with VBA units also displayed digital fluorescence responses to pH variation ($|a|$ = 5.58 ± 0.98; pK_a = 5.09 ± 0.05) in Britton–Robinson buffer solutions at 20 °C (Fig. 4e and S4e). These results indicate the generality of the operational mechanism of digital fluorescent polymeric pH probes with acidic or basic structures as proton-releasing or

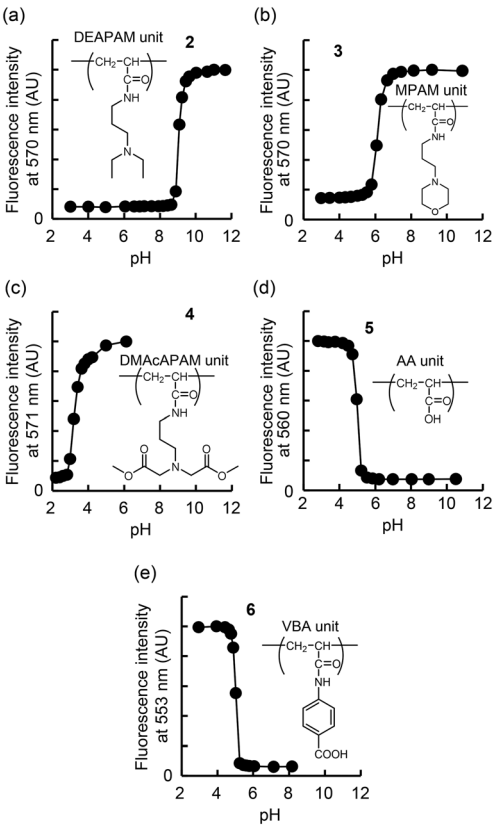

Fig. 4 Modulation of the operational pH range and fluorescence switching direction of digital fluorescent polymeric pH probes. (a–e) Digital fluorescence responses of **2–6** (0.01 w/v%) to pH variations in Britton–Robinson buffer solutions. The indicated chemical structure is the proton-binding unit of each copolymer. Samples were excited at 450 nm. Temperatures were (a) 40 °C, (b) 50 °C, (c) 40 °C, (d) 45 °C and (e) 20 °C.

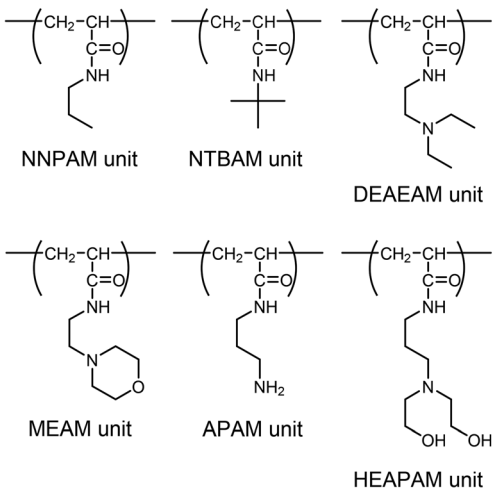

Fig. 5 Chemical structures of monomers for thermoresponsive and proton-binding units.

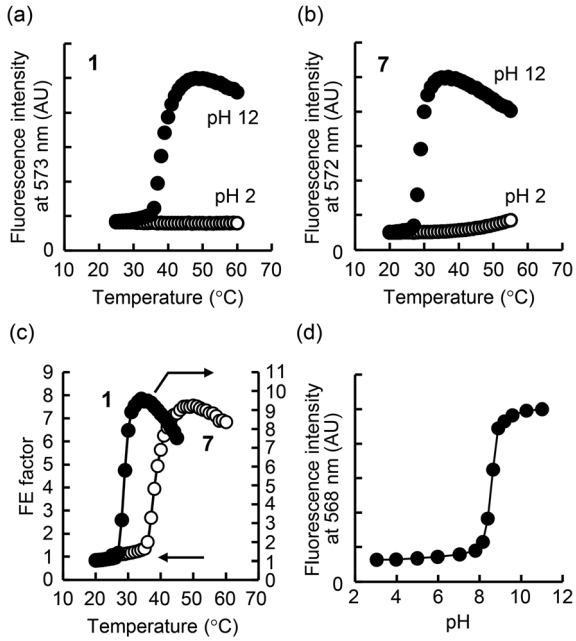

Fig. 6 Comparison of operational temperature ranges of **1** and **7** as digital fluorescent polymeric pH probes. (a and b) Detailed relationships between the fluorescence intensity of (a) **1** and (b) **7** (0.01 w/v%) and temperature in Britton–Robinson buffer solutions at pH 12 (closed) and 2 (open). Samples were excited at 450 nm. (c) Fluorescence enhancement factors of **1** (open) and **7** (closed). Using the data shown in panels (a) and (b), the fluorescence intensity at pH 12 was divided by that at pH 2 at each temperature. (d) Digital fluorescence response of **7** (0.01 w/v%) to pH variations during excitation at 450 nm in Britton–Robinson buffer solutions at 37 °C.

receiving moieties. The fluorescence properties of copolymers **2–6** are summarized in Table 3.

Modulation of the operational temperature of digital fluorescent polymeric pH probes

Next, we investigated the effect of thermoresponsive units on the copolymer's function to tune the operational temperature range. We prepared copolymers **7** and **8**, containing NNPAM and NTBAM units (Fig. 5), respectively (Table 1). The phase transition temperatures of NIPAM and NNPAM homopolymers in water are 31 °C and 22 °C, respectively, while the NTBAM homopolymer is too hydrophobic to dissolve in water, even at 0 °C.[56] Fig. 6a and b display the detailed temperature-dependent fluorescence intensity of **1** and **7** at pH 2 and 12, respectively. The fluorescence enhancement factors of **1** and **7** (Fig. 6c) indicate that the operational temperature range of **7** is lower than that of **1**. Despite changing the thermoresponsive units, the digital behavior of the fluorescence response to pH variation was maintained in **7** (a = 2.78 ± 0.39; pK_a = 8.58 ± 0.02) in Britton–Robinson buffer solutions at 37 °C (Fig. 6d). This result suggests that **7** is more suitable for experiments with mammalian cells than **1** in terms of an operational temperature range, although further tuning might be required for the function in the physiological pH range. The fluorescence properties of **7** are summarized in Table 3. However, the highly hydrophobic NTBAM prevents **8** from adopting an open form,

even at pH 2 (Fig. S5). Nevertheless, moderate fluorescence switching can be observed by varying the pH from 2 to 12 at a low temperature (5 °C). The phase transition temperature of a thermoresponsive polymer can be more precisely tuned by mixing two thermoresponsive units.[57] Thus, the functional temperature range of a digital fluorescent polymeric pH probe can be arbitrarily tuned by choosing appropriate thermoresponsive units.

Additional relations between the chemical structures of components and the function of fluorescent copolymers

Apart from the fluorescent copolymers described herein, we synthesized additional fluorescent copolymers comprising various ratio of different units. Most of the experimental procedures and functional data of these copolymers are summarized in the SI.

The effect of the unit ratio (thermoresponsive NIPAM unit : proton-binding DMAPAM unit) in poly(NIPAM-*co*-DMAPAM-*co*-DBD-AA) was investigated. **1** and copolymers **S1–S6** were prepared with different NIPAM : DMAPAM ratios in the feed solution (Table S3). The actual composition ratios of NIPAM and DMAPAM units in **S1–S6** were essentially the same as those of the corresponding monomers in the feed. The temperature-dependent fluorescence intensity of **1** and **S1–S6** at pH 2 and 12 (Fig. 2a and S6) indicates that the optimized NIPAM : DMAPAM ratio in the feed is 90 : 10, resulting in a wide functional temperature range where significant fluorescence enhancement is observed owing to pH variations. This was also confirmed for poly(NIPAM-*co*-MPAM-*co*-DBD-AA) by preparing **S7** with an 80 : 20 NIPAM : MPAM ratio in the feed and comparing its fluorescence response with **2** (Fig. 4b and S7). Therefore, we fixed the monomer ratio in the feed for thermoresponsive and proton-binding units as 90 : 10 herein.

Next, we investigated the effects of the length of a methylene chain of proton-binding units. Copolymers **S8** and **S9** comprising *N*-[2-(diethylamino)ethyl]acrylamide (DEAEAM) and *N*-(2-morpholinoethyl)acrylamide (MEAM) units (Fig. 5) with ethylene chains instead of propylene chains of DEAPAM and MPAM units in **2** and **3**, respectively, were prepared (Table S3). The fluorescence responses of **S8** and **S9** (Fig. S8) are not significantly different from those of **2** and **3**, indicating that the methylene chain length in pH-responsive units does not have a remarkable effect on the function of digital fluorescent pH probes.

Finally, for practical applications using digital fluorescent pH probes, the limitations of our polymeric design were investigated. Copolymers **S10** and **S11** comprising APAM and *N*-{3-[bis(2-hydroxyethyl)amino]propyl}acrylamide (HEAPAM) units (Fig. 5), respectively, were prepared (Table S3). The fluorescence responses of **S10** and **S11** (Fig. S9) indicated that they failed to function as digital fluorescent polymeric pH probes. **S10** exhibits heat-induced fluorescence enhancement, even at pH 2, likely because of the insufficient hydrophilicity of the protonated monoalkyl amino group in the APAM units. At a selected temperature (40 °C), although moderate pH-dependent fluorescence switching occurs, it was not as sharp as that of digital fluorescent pH probes (Fig. S9a; a = 0.82; pK_a = 9.32). Additionally, **S11** did not exhibit a digital-type response (a = 0.99 ± 0.03; pK_a = 7.40 ± 0.08), although fluorescence off–on switching occurred by varying pH at 50 °C (Fig. S9b). The operational behavior of **S11** is likely because of hydroxy groups in HEAPAM units, which increase local hydrophilicity and disable the operational mechanism of digital fluorescent polymeric pH probes.

Molecular logic operation using a digital fluorescent pH probe in an aqueous solution and live cells

Considering that the developed digital fluorescent polymeric pH probes have the sensing ability to temperature variation, their function is utilized as a fluorescent logic gate,[17–20] which can simultaneously sense two or more chemical/physical factors and distinguish complex environmental conditions. The practical applications of molecular logic gates have been extended to the molecular computational identification of small objects[58] and medical science (diagnostics[59] and therapy[60,61]). As an application of the as-prepared probe, an intracellular logic operation using copolymer **9** (Fig. 7a) comprising thermoresponsive NIPAM, proton-binding MPAM and fluorescent DBD-AA units was explored. Compared with **3** comprising identical units, **9** possessed substantially more DBD-AA units for live-cell imaging *via* fluorescence microscopy.

The function of **9** as a fluorescent polymeric logic gate was evaluated in Britton–Robinson buffer solutions under four different pH and temperature conditions using a spectrofluorometer (Fig. 7b) and a TCSPC fluorescence lifetime spectro-

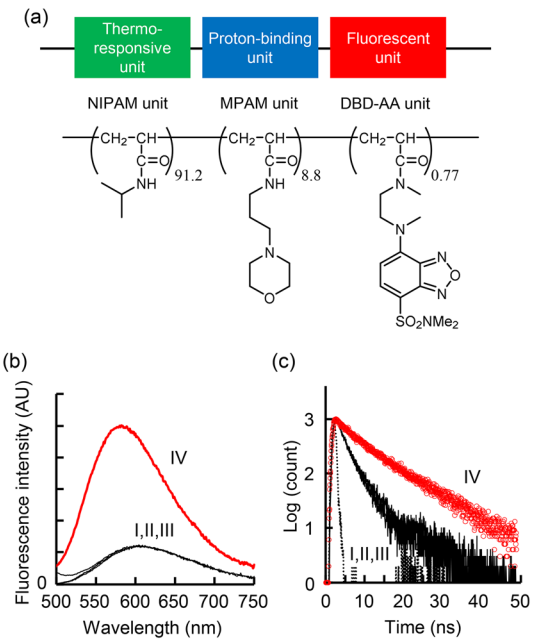

Fig. 7 AND logic operation using **9** in Britton–Robinson buffer solutions. (a) Chemical structure of **9**. (b and c) Fluorescence spectra (0.001 w/v%, excited at 450 nm) (b), and fluorescence decay curves (0.02 w/v%, excited at 456 nm and emission collected over 500 nm) (c) of **9** under four different pH and temperature conditions (I–IV, see Table 4).

Table 4 Truth table and fluorescence properties of **9** in Britton–Robinson buffer solutions

Condition	Input$_1$ (pH)	Input$_2$ (T)	Output (RFI, τ_f [a])	λ_{em} [b]/nm	Φ_f	$k_f/10^7$ s^{-1}	$k_{nr}/10^7$ s^{-1}
I	0 (2)	0 (20 °C)	0 (0.18, 2.7 ns)	604	0.046	1.7	35.3
II	1 (12)	0 (20 °C)	0 (0.19, 3.2 ns)	604	0.054	1.7	30.0
III	0 (2)	1 (40 °C)	0 (0.19, 2.7 ns)	604	0.050	1.9	34.9
IV	1 (12)	1 (40 °C)	1 (1.0, 8.3 ns)	580	0.21	2.6	9.5

[a] Average fluorescence lifetimes at λ_{em}. Calculated using double-exponential components (Table S4) and eqn (7). [b] Excited at 450 nm and corrected.

meter (Fig. 7c): pH (input$_1$) was set at 2 (low, input$_1$ = 0) or 12 (high, input$_1$ = 1), and the temperature (input$_2$) was set at 20 °C (low, input$_2$ = 0) or 40 °C (high, input$_2$ = 1). A strong fluorescence with long fluorescence decay occurs only when pH and temperature are high. As summarized in a truth table showing the input–output pattern (Table 4), the outputs of **9** (fluorescence intensity and lifetime) are switched on when both inputs are high and switched off under the other conditions. The response pattern of **9** corresponds to an AND logic gate. Notably, the extremely sharp responses of **9** to pH and temperature variations enable effective logic operations because such distinguishable output states with slight input differences are crucial for accurate performance, especially in decision making in medical applications[62] and sequential input–output communication between multiple molecules.[63,64]

Finally, we used **9** to perform a logic operation inside live cells. Although intracellular logic operation is an appealing application of fluorescent logic gates, its realization has been limited for a long time.[65,66] Nevertheless, the number of reports on intracellular logic operations has increased significantly within the past five years,[67,68] primarily because of their importance, especially in medicine.[69,70] Multiplex sensory molecules that can simultaneously monitor multiple chemical/physical parameters in different output modes[31,71] are accelerating this trend. The inputs (pH and temperature) of **9** are endogenous chemical and physical parameters of live cells. The fluorescent polymeric logic gate **9** was smoothly incorporated into live HeLa cells from a culture medium by treatment at room temperature for 10 min. Cationizable MPAM units facilitated the spontaneous entry of **9** into living cells through the plasma membrane.[72] After the incorporation, **9** remained in the cytoplasm without leaking. To evaluate the logic operation of **9** in live cells, bright-field (BF) and fluorescence lifetime images of live HeLa cells with **9** were recorded under four different pH (5.5 (low) and 8.0 (high)) and temperature (22 °C (low) and 37 °C (high)) conditions (Fig. 8). In these cellular experiments, intracellular pH and temperature were controlled by nigericin-containing phosphate buffer solutions[41] and a stage heater, respectively. In live cell imaging, the exact intracellular concentration of a fluorescent probe cannot be determined because the cell size varies. Therefore, probe concentration–independent fluorescence lifetime is a more suitable detection parameter than fluorescence intensity in fluorescence cell imaging.[73]

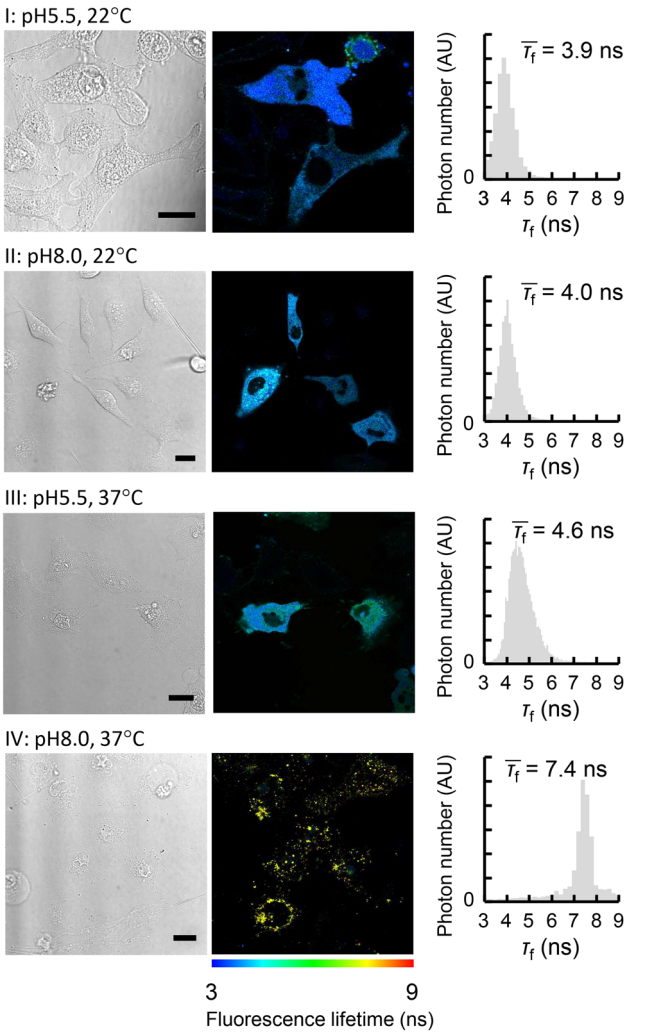

Fig. 8 AND logic operation by copolymer **9** in living HeLa cells. Bright-field images (left), fluorescence lifetime images (excited at 470 nm and emission collected between 500 and 700 nm) (middle) and histograms of fluorescence lifetime in a representative cell (right) under four different intracellular pH and temperature conditions (I–IV). $\overline{\tau_f}$ represents the average of the histogram. Scale bars represent 20 μm.

Among four different conditions, an extended fluorescence lifetime (>7 ns) was observed at high pH (8.0) and high temperature (37 °C), as summarized in the truth table for **9** in HeLa cells (Table 5). The three-dimensional structural change in **9** to hydrophobic globules during the operation at high pH and

Table 5 Truth table for **9** in living HeLa cells

Condition	Input$_1$ (pH)	Input$_2$ (T)	Output ($\overline{\tau_f}$ [a])
I	0 (5.5)	0 (22 °C)	0 (3.8 ± 0.16 ns)
II	1 (8.0)	0 (22 °C)	0 (4.0 ± 0.03 ns)
III	0 (5.5)	1 (37 °C)	0 (4.5 ± 0.37 ns)
IV	1 (8.0)	1 (37 °C)	1 (7.4 ± 0.12 ns)

[a] Average fluorescence lifetime in a single cell. Average ± s.d. for 3–8 cells.

temperature inside HeLa cells with high ionic strength was verified based on moderate aggregation of **9** (recognized as dots in the fluorescence lifetime image in case IV; Fig. 8) and extension of the fluorescence lifetime. As confirmed in Fig. S10, the AND function of **9** within cells was achieved through small variations in intracellular pH and temperature. Thus, the digital polymeric pH probe-based logic gate **9** is superior to conventional small molecule-based AND logic gates because it can produce a definite output response with slight input variations. Such efficient switching is a significant advantage of our polymeric design of a fluorescent logic gate, which enables solid molecular computation, even within biological milieus, where environmental fluctuations are restricted. Our results pave the way for the next stage of intracellular molecular computation, where the intelligence of chemical logic operations is combined with the elaborateness of biological fields to create new science.

Conclusions

We designed fluorescent polymeric digital pH probes comprising thermoresponsive, proton-binding, and environment-sensitive fluorescent units. The ultimate response efficiency of digital pH probes based on fluorescence switching achieved by a slight difference in proton concentrations was enabled using a polymeric design involving local hydrophobicity variation during operation. Similar sharp responses were observed in the hydrophobic effect-induced cooperativity of protein–ligand complexation.[74,75] Thus, we assumed that macromolecules in an aqueous solution could exploit the change in local hydrophobicity to acquire indispensable sensitivity and selectivity in molecular recognition. However, their synthetic costs are significantly higher than those for small molecules. As the next steps for fluorescent digital probes, we will perform highly sensitive pH monitoring of real samples (water and biological cells) and extend the detection target to alkaline (Na^+ or K^+) ions, exploiting the flexibility of polymeric design.

Author contributions

S. U.: writing – original draft, visualization, project administration, investigation, funding acquisition, data curation, conceptualization. E. H.: investigation. M. T.: investigation. K. O.: writing – review & editing, investigation.

Conflicts of interest

There are no conflicts to declare.

Data availability

Data for this study are available from UTokyo Repository at https://r.dl.itc.u-tokyo.ac.jp/esploro/outputs/9913110009301.

Supplementary information (SI) is available. See DOI: https://doi.org/10.1039/d5an01187f.

Acknowledgements

We dedicate this paper to Prof. Amilra Prasanna de Silva in sincere appreciation for his pioneering work in establishing molecular logic gates and for his continuous, engaging discussions, even after the closure of his laboratory at Queen's University Belfast in 2022. We thank Dr M. Shibata and Ms. M. Okada (HORIBA, Ltd) for valuable instruction in pH measurements of mixed solvents. S. U. thanks Japan Society for the Promotion of Science (Grant-in-Aid for Challenging Exploratory Research, No. 24655059), Foundation for Promotion of Material Science and Technology of Japan, Ogasawara Foundation for the Promotion of Science and Engineering, and Iketani Science and Technology Foundation (No. 0251023-A) for financial support.

References

1 A. P. de Silva, H. Q. N. Gunaratne, T. Gunnlaugsson, A. J. M. Huxley, C. P. McCoy, J. T. Rademacher and T. E. Rice, Signaling recognition events with fluorescent sensors and switches, *Chem. Rev.*, 1997, **97**, 1515–1566.
2 K. P. Carter, A. M. Young and A. E. Palmer, Fluorescent sensors for measuring metal ions in living systems, *Chem. Rev.*, 2014, **114**, 4564–4601.
3 S.-H. Park, N. Kwon, J.-H. Lee, J. Yoon and I. Shin, Synthetic ratiometric fluorescent probes for detection of ions, *Chem. Soc. Rev.*, 2020, **49**, 143–179.
4 J. Han and K. Burgess, Fluorescent indicators for intracellular pH, *Chem. Rev.*, 2010, **110**, 2709–2728.
5 R. P. Bell, *The proton in chemistry*, Cornell University Press, New York, 1959.
6 F. M. Harold, *The vital force: a study of bioenergetics*, Freeman, New York, 1986.
7 J.-T. Hou, W. X. Ren, K. Li, J. Seo, A. Sharma, X.-Q. Yu and J. S. Kim, Fluorescent bioimaging of pH: from design to applications, *Chem. Soc. Rev.*, 2017, **46**, 2076–2090.
8 The change in ICT characteristics is also involved in ratiometric fluorescent probes such as seminaphtorhodafluor-1 (SNARF-1). See; O. Seksek, N. Henry-Toulmé, F. Sureau and J. Bolard, SNARF-1 as an intracellular pH indicator in laser microspectrofluorometry: a critical assessment, *Anal. Biochem.*, 1991, **193**, 49–54.

9 G. Gabor and D. R. Walt, Sensitivity enhancement of fluorescent pH indicators by inner filter effects, *Anal. Chem.*, 1991, **63**, 793–796.
10 K. Zhou, Y. Wang, X. Huang, K. Luby-Phelps, B. D. Sumer and J. Gao, Tunable, ultrasensitive pH-responsive nanoparticles targeting specific endocytic organelles in living cells, *Angew. Chem., Int. Ed.*, 2011, **50**, 6109–6114.
11 K. Zhou, H. Liu, S. Zhang, X. Huang, Y. Wang, G. Huang, B. D. Sumer and J. Gao, Multicolored pH-tunable and activatable fluorescence nanoplatform responsive to physiologic pH stimuli, *J. Am. Chem. Soc.*, 2012, **134**, 7803–7811.
12 X. Ma, Y. Wang, T. Zhao, Y. Li, L.-C. Su, Z. Wang, G. Huang, B. D. Sumer and J. Gao, Ultra-pH-sensitive nanoprobe library with broad pH tunability and fluorescence emissions, *J. Am. Chem. Soc.*, 2014, **136**, 11085–11092.
13 I. V. Nesterova and E. E. Nesterov, Rational design of highly responsive pH sensors based on DNA i-motif, *J. Am. Chem. Soc.*, 2014, **136**, 8843–8846.
14 X. Luo, H. Yang, H. Wang, Z. Ye, Z. Zhou, L. Gu, J. Chen, Y. Xiao, X. Liang, X. Qian and Y. Yang, Highly sensitive Hill-type small-molecule pH probe that recognizes the reversed pH gradient of cancer cells, *Anal. Chem.*, 2018, **90**, 5803–5809.
15 Y. Xiao, F. Hu, X. Luo, M. Zhao, Z. Sun, X. Qian and Y. Yang, Modulating the pK_a values of Hill-type pH probes for biorelevant acidic pH range, *ACS Appl. Bio Mater.*, 2021, **4**, 2097–2103.
16 F. Hu, Y. Huang, Y. Xiao, Y. Li, X. Luo, X. Qian and Y. Yang, A dual-channel Hill-type small-molecule pH probe, *Anal. Methods*, 2021, **13**, 3012–3016.
17 A. P. de Silva and S. Uchiyama, Molecular logic and computing, *Nat. Nanotechnol.*, 2007, **2**, 399–410.
18 A. P. de Silva, *Molecular logic-based computation*, Royal Society of Chemistry, Cambridge, 2013.
19 S. Erbas-Cakmak, S. Kolemen, A. C. Sedgwick, T. Gunnlaugsson, T. D. James, J. Yoon and E. U. Akkaya, Molecular logic gates: the past, present and future, *Chem. Soc. Rev.*, 2018, **47**, 2228–2248.
20 C.-Y. Yao, H.-Y. Lin, H. S. N. Crory and A. P. de Silva, Supramolecular agents running tasks intelligently (SMARTI): recent developments in molecular logic-based computation, *Mol. Syst. Des. Eng.*, 2020, **5**, 1325–1353.
21 Y. Wang, K. Zhou, G. Huang, C. Hensley, X. Huang, X. Ma, T. Zhao, B. D. Sumer, R. J. DeBerardinis and J. Gao, A nanoparticle-based strategy for the imaging of a broad range of tumours by nonlinear amplification of microenvironment signals, *Nat. Mater.*, 2014, **13**, 204–212.
22 S. Uchiyama and Y. Makino, Digital fluorescent pH sensors, *Chem. Commun.*, 2009, 2646–2648.
23 S. Fujishige, K. Kubota and I. Ando, Phase transition of aqueous solutions of poly(*N*-isopropylacrylamide) and poly (*N*-isopropylmethacrylamide), *J. Phys. Chem.*, 1989, **93**, 3311–3313.
24 H. G. Schild, Poly(*N*-isopropylacrylamide): experiment, theory and application, *Prog. Polym. Sci.*, 1992, **17**, 163–249.
25 N. A. Shaibie, N. A. Ramli, N. D. F. M. Faizal, T. Srichana and M. C. I. M. Amin, Poly(*N*-isopropylacrylamide)-based polymers: recent overview for the development of temperature-responsive drug delivery and biomedical applications, *Macromol. Chem. Phys.*, 2023, **224**, 2300157.
26 M. Irie, Y. Misumi and T. Tanaka, Stimuli-responsive polymers: chemical induced reversible phase separation of an aqueous solution of poly(*N*-isopropylacrylamide) with pendent crown ether groups, *Polymer*, 1993, **34**, 4531–4535.
27 C. Gota, S. Uchiyama and T. Ohwada, Accurate fluorescent polymeric thermometers containing an ionic component, *Analyst*, 2007, **132**, 121–126.
28 S. Uchiyama, *Intracellular thermometry with fluorescent molecular thermometers*, Wiley-VCH, Weinheim, 2024.
29 K. Okabe and S. Uchiyama, Intracellular thermometry uncovers spontaneous thermogenesis and associated thermal signaling, *Commun. Biol.*, 2021, **4**, 1377.
30 Y. Akiyama, K. Yoshizako, Y. Hasegawa and T. Okano, Temperature-responsive polymer compound and process for producing the same, *International Patent* WO 00/44800, Aug 3, 2000.
31 S. Uchiyama, K. Iwai and A. P. de Silva, Multiplexing sensory molecules map protons near micellar membranes, *Angew. Chem., Int. Ed.*, 2008, **47**, 4667–4669.
32 C. Gota, S. Uchiyama, T. Yoshihara, S. Tobita and T. Ohwada, Temperature-dependent fluorescence lifetime of a fluorescent polymeric thermometer, poly(*N*-isopropylacrylamide), labeled by polarity and hydrogen bonding sensitive 4-sulfamoyl-7-aminobenzofurazan, *J. Phys. Chem. B*, 2008, **112**, 2829–2836.
33 Y. Maeda, T. Nakamura and I. Ikeda, Changes in the hydration states of poly(*N*-alkylacrylamide)s during their phase transitions in water observed by FTIR spectroscopy, *Macromolecules*, 2001, **34**, 1391–1399.
34 N. A. A. El-Ghany, M. S. A. Aziz, M. M. Abdel-Aziz and Z. Mahmoud, Antimicrobial and swelling behaviors of novel biodegradable corn starch grafted/poly(4-acrylamidobenzoic acid) copolymers, *Int. J. Biol. Macromol.*, 2019, **134**, 912–920.
35 H. T. S. Britton and R. A. Robinson, Universal buffer solutions and the dissociation constant of veronal, *J. Chem. Soc.*, 1931, 1456–1462.
36 V. E. Bower and R. G. Bates, pH values of the Clark and Lubs buffer solutions at 25 °C, *J. Res. Natl. Bur. Stand.*, 1955, **55**, 197–200.
37 G. Gomori, Preparation of buffers for use in enzyme studies, *Methods Enzymol.*, 1955, **1**, 138–146.
38 G. Gottschalk, Tartrat- und citratpuffer, *Fresenius' Z. Anal. Chem.*, 1961, **183**, 420–426.
39 R. G. Bates, M. Paabo and R. A. Robinson, Interpretation of pH measurements in alcohol-water solvents, *J. Phys. Chem.*, 1963, **67**, 1833–1838.
40 R. G. Bates, *Determination of pH. Theory and practice*, John Wiley & Sons, New York, 1973, pp. 243–249.
41 B. A. Webb, F. M. Aloisio, R. A. Charafeddine, J. Cook, T. Wittmann and D. L. Barber, pHLARE: a new biosensor

reveals decreased lysosome pH in cancer cells, *Mol. Biol. Cell*, 2021, **32**, 131–142.

42 The Britton–Robinson buffer was primarily used in this study due to its universal characteristic for a wide pH range from 2 to 12. The pH values indicated in this paper were all measured at 20 °C and uncorrected. The pH values of the Britton–Robinson buffer solutions are temperature-dependent, especially in the alkaline region (*i.e.*, 12.0 and 11.1 at 20 and 60 °C, respectively). Nevertheless, the fluorescence properties of our copolymers were not influenced by this temperature-dependent pH variation because the functional pH ranges of our copolymers were out of the region.

43 O. S. Wolfbeis, E. Fürlinger, H. Kroneis and H. Marsoner, Fluorimetric analysis 1. A study on fluorescent indicators for measuring near neutral ("physiological") pH-values, *Fresenius' Z. Anal. Chem.*, 1983, **314**, 119–124.

44 H. N. Po and N. M. Senozan, The Henderson-Hasselbalch equation: its history and limitations, *J. Chem. Educ.*, 2001, **78**, 1499–1503.

45 The sharp fluorescence response of **1** to pH variation was also confirmed in 0.1 M borate buffer solutions (a = 2.76, pK_a = 8.41). See Fig. S11a.

46 M. Y. Berezin and S. Achilefu, Fluorescence lifetime measurements and biological imaging, *Chem. Rev.*, 2010, **110**, 2641–2684.

47 S. Uchiyama, K. Kimura, C. Gota, K. Okabe, K. Kawamoto, N. Inada, T. Yoshihara and S. Tobita, Environment-sensitive fluorophores with benzothiadiazole and benzoselenadiazole structures as candidate components of a fluorescent polymeric thermometer, *Chem. – Eur. J.*, 2012, **18**, 9552–9563.

48 A. P. de Silva, T. S. Moody and G. D. Wright, Fluorescent PET (Photoinduced Electron Transfer) sensors as potent analytical tools, *Analyst*, 2009, **134**, 2385–2393.

49 M. S. K. Niazi and J. Mollin, Dissociation constants of some amino acid and pyridinecarboxylic acids in ethanol-H_2O mixtures, *Bull. Chem. Soc. Jpn.*, 1987, **60**, 2605–2610.

50 A. Avdeef, J. E. A. Comer and S. Thomson, pH-Metric log *P*. 3. Glass electrode calibration in methanol–water, applied to pK_a determination of water-insoluble substances, *Anal. Chem.*, 1993, **65**, 42–49.

51 M. Chiari, C. Ettori and P. G. Righetti, Capillary zone electrophoresis of acrylamido buffers for isoelectric focusing in immobilized pH gradients, *J. Chromatogr.*, 1991, **559**, 119–131.

52 The pK_a value of the conjugate acid of DMAcAPAM was calculated to be 3.4 by ChemDraw® Professional ver. 16.

53 The sharp fluorescence response of **3** to pH variation was also confirmed in 0.2 M phosphate buffer solutions (a = 2.34, pK_a = 5.97). See Fig. S11b.

54 The sharp fluorescence response of **5** to pH variation was also confirmed in 0.2 M citrate buffer solutions ($|a|$ = 2.29, pK_a = 5.40). See Fig. S11c.

55 E. Rossini, A. D. Bochevarov and E. W. Knapp, Empirical conversion of pK_a values between different solvents and interpretation of the parameters: application to water, acetonitrile, dimethyl sulfoxide, and methanol, *ACS Omega*, 2018, **3**, 1653–1662.

56 S. Ito, Phase transition of aqueous solution of poly(*N*-alkylacrylamide) derivatives. Effects of side chain structure, *Kobunshi Ronbunshu*, 1989, **46**, 437–443.

57 S. Uchiyama, Y. Matsumura, A. P. de Silva and K. Iwai, Modulation of the sensitive temperature range of fluorescent molecular thermometers based on thermoresponsive polymers, *Anal. Chem.*, 2004, **76**, 1793–1798.

58 A. P. de Silva, M. R. James, B. O. F. McKinney, D. A. Pears and S. M. Weir, Molecular computational elements encode large populations of small objects, *Nat. Mater.*, 2006, **5**, 787–790.

59 T. Konry and D. R. Walt, Intelligent medical diagnostics via molecular logic, *J. Am. Chem. Soc.*, 2009, **131**, 13232–13233.

60 R. J. Amir, M. Popkov, R. A. Lerner, C. F. Barbas III and D. Shabat, Prodrug activation gated by a molecular "OR" logic trigger, *Angew. Chem., Int. Ed.*, 2005, **44**, 4378–4381.

61 S. Ozlem and E. U. Akkaya, Thinking outside the silicon box: molecular AND logic as an additional layer of selectivity in singlet oxygen generation for photodynamic therapy, *J. Am. Chem. Soc.*, 2009, **131**, 48–49.

62 J. Halámek, J. R. Windmiller, J. Zhou, M.-C. Chuang, P. Santhosh, G. Strack, M. A. Arugula, S. Chinnapareddy, V. Bocharova, J. Wang and E. Katz, Multiplexing of injury codes for the parallel operation of enzyme logic gates, *Analyst*, 2010, **135**, 2249–2259.

63 S. Silvi, E. C. Constable, C. E. Housecroft, J. E. Beves, E. L. Dunphy, M. Tomasulo, F. M. Raymo and A. Credi, All-optical integrated logic operations based on chemical communication between molecular switches, *Chem. – Eur. J.*, 2009, **15**, 178–185.

64 E. T. Ecik, A. Atilgan, R. Guliyev, T. B. Uyar, A. Gumus and E. U. Akkaya, Modular logic gates: cascading independent logic gates *via* metal ion signals, *Dalton Trans.*, 2014, **43**, 67–70.

65 D. P. Murale, H. Liew, Y.-H. Suh and D. G. Churchill, Mercuric-triggered hydrogen peroxide "turn-on" fluorescence detection in neuronal cells with novel fluorescein-based probe obtained in one pot, *Anal. Methods*, 2013, **5**, 2650–2652.

66 I. Takashima, R. Kawagoe, I. Hamachi and A. Ojida, Development of an AND logic-gate-type fluorescent probe for ratiometric imaging of autolysosome in cell autophagy, *Chem. – Eur. J.*, 2015, **21**, 2038–2044.

67 J. Zheng, Q. Wang, L. Shi, P. Peng, L. Shi and T. Li, Logic-gated proximity aptasensing for cell-surface real-time monitoring of apoptosis, *Angew. Chem., Int. Ed.*, 2021, **60**, 20858–20864.

68 Y. Shen, W. Li, Z. Zhou, J. Xu, Y. Li, H. Li, X. Zheng, S. Liu, X.-B. Zhang and L. Yuan, Dual-locked fluorescent probes activated by aminopeptidase N and the tumor redox environment for high-precision imaging of tumor boundaries, *Angew. Chem., Int. Ed.*, 2024, **63**, e202406332.

69 L. Wu, J. Huang, K. Pu and T. D. James, Dual-locked spectroscopic probes for sensing and therapy, *Nat. Rev. Chem.*, 2021, **5**, 406–421.
70 X. Zhang, T. Xiu, H. Wang, H. Wang, P. Li and B. Tang, Recent progress in the development of small-molecule double-locked logic gate fluorescence probes, *Chem. Commun.*, 2023, **59**, 11017–11027.
71 L. Wu, J. Liu, X. Tian, R. R. Groleau, B. Feng, Y. Yang, A. C. Sedgwick, H.-H. Han, Y. Wang, H.-M. Wang, F. Huang, S. D. Bull, H. Zhang, C. Huang, Y. Zang, J. Li, X.-P. He, P. Li, B. Tang, T. D. James and J. L. Sessler, Dual-channel fluorescent probe for the simultaneous monitoring of peroxynitrite and adenosine-5′-triphosphate in cellular applications, *J. Am. Chem. Soc.*, 2022, **144**, 174–183.
72 T. Tsuji, S. Yoshida, A. Yoshida and S. Uchiyama, Cationic fluorescent polymeric thermometers with the ability to enter yeast and mammalian cells for practical intracellular temperature measurements, *Anal. Chem.*, 2013, **85**, 9815–9823.
73 W. Becker, Fluorescence lifetime imaging – techniques and applications, *J. Microsc.*, 2012, **247**, 119–136.
74 D. H. Williams and B. Bardsley, Estimating binding constants – The hydrophobic effect and cooperativity, *Perspect. Drug Discovery Des.*, 1999, **17**, 43–59.
75 L. Jiang, S. Cao, P. P.-H. Cheung, X. Zheng, C. W. T. Leung, Q. Peng, Z. Shuai, B. Z. Tang, S. Yao and X. Huang, Realtime monitoring of hydrophobic aggregation reveals a critical role of cooperativity in hydrophobic effect, *Nat. Commun.*, 2017, **8**, 15639.
76 G. Åkerlöf, Dielectric constants of some organic solvent-water mixtures at various temperatures, *J. Am. Chem. Soc.*, 1932, **54**, 4125–4139.